02

# Structure studies of graded amorphous carbon obtained by liquid carbon quenching

© V.S. Dozhdikov, A.Yu. Basharin, P.R. Levashov

Joint Institute for High Temperatures, Russian Academy of Sciences,
Moscow, Russia
e-mail: vdozh@mail.ru

Received August 16, 2022
Revised January 5, 2023
Accepted January 9, 2023

A new method for obtaining graded amorphous carbon using quenching of a graphite melt on a diamond substrate is proposed. Using molecular dynamics modeling of liquid carbon quenching on a cold diamond substrate, it is shown that the amorphous carbon obtained in the experiment is a material with a strongly gradient structure and properties along the depth of the sample. This is due to the quenching rate decrease with the distance from the substrate in the range of $10^{14}-10^{12}$ K/s. In this case, the density of amorphous carbon varies from 1.50 g/cm$^3$ to 1.93 g/cm$^3$. The spatial change in the structural characteristics of the obtained amorphous carbon was studied: the distribution of carbon atoms according to the degree of chemical bond hybridization ($sp^1$-, $sp^2$-, $sp^3$-), the radial distribution function, the angular distribution function, and a statistical analysis of carbon rings were carried out. It is shown that at a pressure in liquid of 1 GPa, the carbon structure within the quenched zone changes from a highly porous structure with a large number of $sp^1$ chains of carbon atoms near the substrate to an amorphous graphene structure at the periphery.

**Keywords:** amorphous carbon, liquid carbon, quenching, molecular dynamics, radial distribution function.

DOI: 10.21883/TP.2023.03.55804.206-22

## Introduction

The relevance of the study of amorphous carbon ($a$-C), is in no doubt due to the unique properties of such materials [1–6]. The unique properties of $a$-C are largely determined by the fact that it is a „mixture“ of carbon atoms with different types of chemical bond hybridization: $sp^3$-, $sp^2$-, $sp^1$-. And its properties strongly depend on the quantitative ratio between different types of hybridization. Especially many efforts of researchers worldwide are focused on studying the properties of dense, diamond-like $a$-C with a high content of atoms with $sp^3$ hybridization [5]. Describing and understanding the structure of disordered or amorphous carbon are not easy, because such materials do not have a definite crystal lattice [7]. Therefore, $a$-C model structures created by computer simulation methods are of exceptional importance for understanding how such complex structures are formed in actual processes or experiments, how to optimize these processes and achieve the desired properties of $a$-C.

Graded materials with a continuous spatial change in structure and properties are used in various technologies. The concept of graded (functionally graded) materials utilization in industry first occurred in Japan in the 80s [8] for application in space engineering. In recent years, this direction continues active development, and graded materials are used in the aerospace and automotive industries, in power engineering, microelectronics, and in the design of various structures [9]. Graded materials are usually used when properties are required that are not available in conventional technical materials. The authors are unaware of publications relating to the creation of graded material based on amorphous carbon.

To obtain new, including amorphous materials with unique properties, quenching from the liquid state is widely used [1,10,11]. The authors managed to carry out unique experiments [12], in which liquid carbon is quenched on the surface of a cold diamond substrate forming the graded $a$-C. The small amount of $a$-C obtained does not allow us to apply the instrumental approach to study its structure. Therefore, it was necessary to involve modeling methods. At the first stage we carried out molecular dynamics (MD) calculations [13,14], where we tried to simulate directly the liquid carbon quenching on the cold diamond substrate in a two-layer modeling cell. But the geometric size of the modeling cells in the calculations did not allow us to reproduce the carbon structures obtained in our experiments, since they were far from the actual sizes of the experimental samples [12]. Besides, in these calculations it was impossible to estimate the rate of the liquid carbon quenching in the experiment, and, as it is known [1], the quenching rate is one of the determining parameters in the formation of amorphous carbon and strongly affects its properties.

In the paper [12], by solving the problem of non-stationary conductive heat transfer for a model that uses the actual sizes of the samples participating in the experiment, it was possible to estimate the rates of the liquid carbon quenching on the cold diamond substrate. The rate of liquid carbon quenching varied depending on the distance

from the diamond–liquid carbon interface. At a distance of $0.005\,\mu$m the quenching rate was maximum — $10^{14}$ K/s, then at a distance of $0.02\,\mu$m it decreased to $10^{13}$ K/s, and further while moving away from the interface at distances greater than $0.05\,\mu$m the quenching rate reached the lowest value $10^{12}$ K/s. Thus, it became possible to simplify the modeling process by excluding the diamond substrate from the modeling cell.

In the present paper, model structures of $a$-C are obtained by the MD quenching of liquid carbon at known rates of quenching. A detailed study of the structural properties of these model samples was carried out. We suppose that these properties are close to those of the carbon structures obtained in the experiment [12].

## 1. MD methods for obtaining amorphous carbon

Although there are different methods for modeling amorphous systems [1], one of the most popular methods for computer simulation of amorphous carbon is MD quenching of liquid carbon [1,15–35]. The liquid carbon quenching involves liquid carbon cooling at high rate to a solid amorphous state. In 1989 the authors [15] published a pioneering work in which amorphous carbon was obtained using *ab initio* MD simulation to quench the liquid carbon at a quenching rate of $10^{16}$ K/s. In the following years and up to the present, not only *ab initio* modeling [17–19,33,35], but also tight-binding modeling [16,19,20,24] and modeling using various (often very complex) potentials [19,21–23,25–34] were used for MD simulation. Separately, we can highlight the papers [27,28], whose authors developed a machine-learning Gaussian approximation potential (GAP). The GAP potential, apparently, has great prospects, since, on the one hand, using an appropriate learning technique it can accurately describe sufficiently large disordered systems, and on the other hand, it is by several orders of magnitude faster than *ab initio* modeling.

There is a certain compromise when choosing a method describing the forces of interaction between atoms in the MD modeling of liquid carbon quenching. On the one hand, *ab initio* modeling gives the most accurate result, but today it does not allow modeling of large systems of atoms. On the other hand, the use of interaction potentials, even in the form of rather complex functionals, makes it possible to model large systems, but, obviously, it is less accurate than *ab initio* methods. Mainly in connection with this, in recent years questions were actively studied [23,25,30–34,36], how to use the potentials in the best possible way, what potentials are best used under certain conditions of modeling of liquid carbon quenching with formation of various carbon structures, what criteria are best used when choosing potentials. The authors [25,32] have been doing a great work to systematize the potentials that exist today for modeling various forms of carbon. But, unfortunately, the general conclusion for today is that it is impossible to select any universal potential for the analysis of various disordered carbon structures [32]. Besides, the authors of paper [33] noted that some structural characteristics of amorphous carbon (for example, the content of carbon rings) cannot be obtained experimentally at all, and data on those characteristics that are determined experimentally (for example, the content of $sp^3$-atoms) are quite rare. This, of course, complicates the procedure for assessing the reliability of a particular potential. Therefore, in order to increase confidence in the results of modeling of liquid carbon quenching using one or another potential, it is necessary to first analyze how adequately the selected potential describes disordered amorphous (and possibly liquid) carbon under the chosen modeling conditions.

It was shown in [37] that the quenching rates commonly used in MD modeling are consistent with experiments on the deposition of thin amorphous carbon films during graphite sputtering and are about $10^{16}$ K/s. In almost all papers [15–35] the liquid carbon was quenched at rates of $10^{15}-10^{16}$ K/s at a constant density of the modeling cell. Thus, during the modeling the number of particles and the cell volume remained unchanged: $N, V = \text{const}$. After quenching $a$-C was usually annealed in one way or another, then compared with the available structural experimental data, and new structural or mechanical properties of $a$-C were calculated. At such high quenching rates, the structure of amorphous samples obtained by MD quenching agrees quite well with the structure of industrial amorphous films obtained, for example, by magnetron sputtering. In some papers [16,20,24,26,33], for whatever reason quenching was carried out at rather „low“ rates of about $10^{13}-10^{14}$ K/s. In the paper [29] to generate an atomic model of highly porous $a$-C carbon obtained from carbides the liquid carbon was quenched at rates of $10^{12}$, $10^{13}$, $10^{14}$ K/s. Basically, the linear law of temperature change during quenching is used, but in a number of papers [18,19,23,26,27,33] the liquid carbon quenching occurs according to an exponential law. Both the quenching rate and the law of temperature change during quenching affect the process itself and the properties (structure) of the resulting $a$-C. But subsequent $a$-C annealing can naturally reduce this effect. In the paper [26] the influence of liquid carbon quenching conditions on $a$-C structure obtained is studied in great detail: quenching rate, type of quenching (linear or exponential cooling law), annealing time, size of modeling cell.

As noted above, quenching takes place at a constant density and, of course, the properties (structure) of the resulting $a$-C depend very strongly on this parameter. Generally modeling of liquid carbon quenching is carried out in the density range from a value close to the graphite density ($sp^2$-atoms) — $2\,\text{g/cm}^3$ to a value close to the diamond density ($sp^3$-atoms) — $3.5\,\text{g/cm}^3$. However, in some papers, the „low“ density $< 2.0\,\text{g/cm}^3$ liquid carbon quenching is studied: in the paper [33] up to $1.7\,\text{g/cm}^3$, in papers [25,27,32] up to $1.5\,\text{g/cm}^3$, in papers [31] up to $1.4\,\text{g/cm}^3$, in paper [20] up to $1.2\,\text{g/cm}^3$, in paper [29] up to $0.95\,\text{g/cm}^3$, in paper [35] up to $0.923\,\text{g/cm}^3$, in paper [24]

up to 0.6 g/cm$^3$, in the paper [26] up to 0.5 g/cm$^3$. When such carbon is quenched, porous structures with cavities having complex shape are obtained, they contain mainly carbon atoms with $sp^1$- and $sp^2$-hybridization. This class of carbon materials is sometimes called disordered nanoporous carbon [38–40]. Highly porous $a$-C carbon obtained from carbides [29] belongs to the same class. Interest in highly porous $a$-C structures is due to their use in water treatment, in electrochemistry (batteries), for the absorption of gases (for example, hydrogen).

## 2. Formulation of the problem of MD quenching

As it was already discussed, in the papers [15–35] in the overwhelming majority of cases the authors simulate quenching at a constant density ($N, V = \text{const}$), then anneal $a$-C and compare the structure and properties of $a$-C either with the experiment or with a more precise calculation *ab initio*. At the same time, in many papers the conditions for liquid carbon quenching (quenching rate, type of quenching, annealing time) are optimized in order to obtain $a$-C with a structure as close as possible to the structure obtained experimentally. Our formulation of the problem of MD modeling of liquid carbon quenching is somewhat different. We are interested in understanding what $a$-C structure could be obtained in actual experiment by quenching a thin layer of liquid carbon on a cold diamond substrate. Therefore, for MD modeling we used the $NPT$ ensemble describing the system equilibrium at a fixed number of particles $N$, constant pressure $P$ and temperature $T$, and the quenching rate from calculations at the macrolevel [12], assuming that this rate is close to the actual quenching rate in the experiment. In the $NPT$ ensemble the density of liquid carbon can change during the modeling, as in actual experiment. To maintain a constant pressure in the Nose–Hoover barostat, the dynamic correction of the dimensions of the modeling cell is carried out. In other words, the target pressure of the barostat when integrating the equations of motion is achieved either by mechanical relaxation or by mechanical compression of $a$-C during modeling. Thus, our calculations were as close as possible to the quenching process in the actual experiment.

Considering the experience of authors [23,25,30–34], we tried to choose the potential for MD modeling very carefully [41]. When choosing a method describing the forces of interaction between atoms in MD modeling, we choose the classical potential use. This was due to the fact that in our calculations the density of liquid carbon at a pressure of 1 GPa was $< 2.0$ g/cm$^3$ [41]. And, as noted in the paper [26], in MD modeling of low-density liquid carbon quenching it is better to use a sufficiently large modeling cell to calculate structural properties, which is still difficult to do for *ab initio* calculations. To solve the problem, it was necessary to choose a classical potential that adequately describes disordered liquid carbon from the point of view of the equation of state in order to correctly describe density changes during quenching in the $NPT$ ensemble. On the other hand, it is important that, in addition, the potential should adequately describe $a$-C structure. The choice of the potential was based on comparison of the results of calculations by the quantum and classical MD methods. Of the six empirical potentials considered in [41], only one potential — ReaxFF-lg [42] — showed good agreement with quantum MD calculations as for the equation of state and for the distribution of carbon atoms with different hybridizations ($sp^1$-, $sp^2$-, $sp^3$-) in liquid carbon at pressures of about 1 GPa.

The ReaxFF-lg potential belongs to the family of reactive bond-order potentials ReaxFF, which were developed to model chemically active complex systems [43]. The authors [23] believe that for ReaxFF potential the $a$-C structure obtained by MD quenching is in good agreement with the experimental and DFT (Density Functional Theory) data at densities $< 2.6$ g/ cm$^3$. In the paper [25] 6 potentials for liquid carbon quenching were analyzed from the point of view of describing the structure of the resulting $a$-C, and it was noted that ReaxFF is one of the potentials working well at low densities. The authors [32] concluded that ReaxFF potential is one of the best potentials for modeling large carbon systems over rather long time.

The parameters of the MD calculation of liquid carbon quenching were as follows. The initial cubic modeling cell with periodic boundary conditions contained 11 408 atoms of liquid carbon at a temperature of 6000 K and pressure of 1.0 GPa. In the paper [41] the lowest pressure of liquid carbon modeling was 1.0 GPa. As it was discussed in detail in [41], modeling at pressures below 1.0 GPa due to large pressure fluctuations during the calculations and the lack of accurate data on the liquid–vapor equilibrium line in the carbon phase diagram can lead to the occurrence of spatial heterogeneities in the modeling cell. The equations of motion are integrated in the $NPT$ ensemble using the Nose–Hoover thermostat-barostat. The temperature damping time parameter $T_{damp}$ was $100\Delta t$, where $\Delta t$ is the time increment, and the pressure damping time parameter $P_{damp}$ was $1000\Delta t$. Before quenching the liquid carbon was equilibrated at a temperature of 6000 K and was highly diffusive. The calculated self-diffusion coefficient for a pressure of 1.0 GPa was $13 \cdot 10^{-5}$ cm$^2$/s. The calculated self-diffusion coefficient for a pressure of — $10^{-5}$ cm$^2$/s.

The initial size of modeling cell size for pressure 1.0 GPa was $57 \times 57 \times 57$ Å. When using ReaxFF potentials, the time increment, especially at high temperatures, should be approximately by order of magnitude smaller than the increment that is usually used for classical MD modeling — 1 fs [44]. Therefore, when integrating the equations of motion we used the time increment 0.1 fs. LAMMPS (Large-Scale Atomic/Molecular Massively Parallel Simulator) software package [45] was used for MD calculation.

MD quenching proceeded at the rates obtained in [12]: $10^{12}$, $10^{13}$ and $10^{14}$ K/s. The temperature varied from 6000

to 300 K according to a linear law. Accordingly, the quenching process lasted 5700, 570, 57 ps. $a$-C obtained after quenching was kept for some time in the $NPT$ ensemble at 300 K. As expected, calculations at the quenching rate of $10^{12}$ K/s turned out to be rather time-consuming.

## 3. Density change during liquid carbon quenching

During quenching the instant density of the modeling cell was calculated. Fig. 1 shows density as a function of temperature, respectively for a pressure of 1.0 GPa for quenching rates $10^{12}$, $10^{13}$ and $10^{14}$ K/s. The presented graphs are approximated by the least squares method using the data obtained in the calculations.

For all quenching rates at the initial stage the density of liquid carbon increases almost linearly with temperature decreasing. For the rate $10^{14}$ K/s there is small non-linearity. Further, liquid carbon amorphization starts, and the density graphs begin to bend, while the rate of density change versus temperature decreases. Finally, approximately at a temperature of 3000 K the density reaches its maximum value. We think that the achievement of the maximum density is associated with the end of the amorphization process. With further decrease in temperature the amorphous carbon relaxes. As can be clearly seen in Fig. 1, the density of amorphous carbon decreases slightly during the relaxation. According to the authors [46] on the basis of the temperature dependence of the root-mean-square displacement of atoms from their initial position during liquid carbon quenching, the temperature 3000 K — is the limiting low temperature at which self-diffusion stops, and liquid carbon is completely converted into amorphous one. Thus, our results, as follows from the analysis of the graphs in Fig. 1, coincide with the conclusions made in the paper [46], and the temperature 3000 K is indeed „critical“ temperature during liquid carbon quenching. In

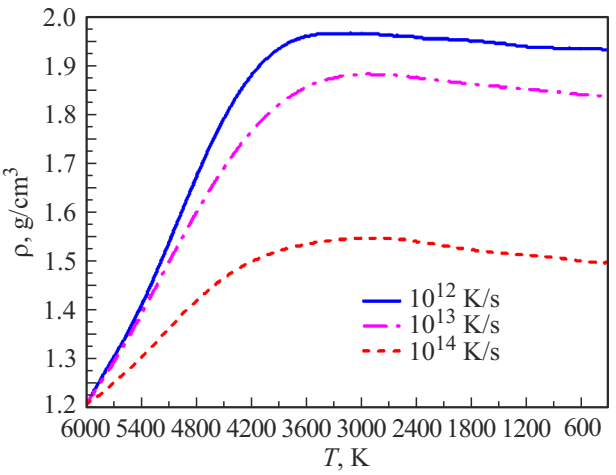


**Figure 1.** The density change of the modeling cell depending on the temperature at different rates of liquid carbon quenching at pressure of 1.0 GPa.

fact, liquid carbon quenching occurs in the range of 6000−3000 K. A further temperature decreasing occurs now in amorphous carbon. The authors [47], carrying out rather thorough calculations of the dependence of the self-diffusion coefficient on temperature during the liquid carbon amorphization, concluded that amorphous carbon exhibits glass-like behavior, this is confirmed by a sharp change in the slope on the graphs for the self-diffusion coefficient in Arrhenius coordinates. In this case, the temperature 3000 K can be interpreted as the glass transition temperature. The graph in Fig. 1 clearly shows that the higher the quenching rate is, the closer the density of $a$-C is to the initial density of liquid carbon. In other words, the higher the quenching rate is, the closer the structure of the obtained $a$-C is to the structure of liquid carbon. At the end of the process the density of $a$-C was: 1.93 g/cm$^3$ for $10^{12}$ K/s , 1.84 g/cm$^3$ for $10^{13}$ K/s, 1.5 g/cm$^3$ for the rate of $10^{14}$ K/s. For all three $a$-C structures obtained the density turned out to be less than the density of graphite — 2 g/cm$^3$. This means that in all three structures the number of atoms with $sp^3$-bond is probably small and, apparently, such structures should be porous, and the lower the density is, the larger the nanopore volume should be.

## 4. Model structures of amorphous carbon

As a result of the MD calculations $a$-C model structures were obtained, which, in our opinion, are quite close in their composition and properties to $a$-C obtained in the experiment. Note that in this paper $a$-C is considered as a condensed substance having a short range atomic order and without long range atomic order characteristic. In Section 4, based on a visual analysis of $a$-C structures, the short range order within the first coordination sphere is studied.

As it was discussed earlier, the distribution of carbon atoms according to the degree of hybridization of the chemical bond is the most important characteristic of $a$-C structure. It is known that the actual distribution cannot be obtained by classical MD modeling methods [48]. Therefore, in the first approximation, as a rule, it is assumed that the degree of hybridization of a carbon atom corresponds to the number of its nearest neighbors. If the atom has 4 neighbors, then it is considered to be coupled with them by the chemical bond of $sp^3$-type, if 3 then this is the chemical bond $sp^2$-, and, finally, for 2 neighbors the chemical bond will be $sp^1$-. The number of neighbors closest to the given atom is calculated within the limits of the short range order within the first coordination sphere, the radius of which is equal to the first minimum of the radial distribution function (RDF).

Fig. 2−4 shows the structures of amorphous carbon obtained at quenching rates $10^{12}$, $10^{13}$ and $10^{14}$ K/s, and the text to the Figures shows the distribution of carbon atoms according to the degree of hybridization of the chemical bond.

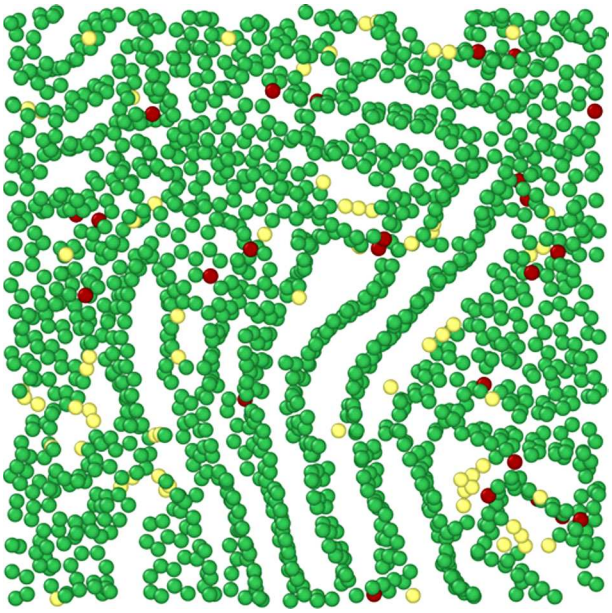

**Figure 2.** Cross section of $a$-C structure for a quenching rate $10^{12}$ K/s. The structure contains 1.6% of atoms with $sp^3$-, 95% of atoms with $sp^2$-, 3.4% of atoms with $sp^1$-hybridization.

For the convenience of visual analysis these Figures show transverse sections 7 Å thick. The atoms of light yellow, green, and maroon colors indicate, respectively, the type of hybridization of the chemical bond $sp^1$-, $sp^2$-, $sp^3$-. Fig. 2, obtained at a relatively low quenching rate $10^{12}$ K/s, shows that $a$-C structure is formed from chaotically mixed and curved graphene-like layers of $sp^2$-atoms (95%). Such a curvature indicates the presence of defects in them, since ideal graphene layers, consisting of hexagons with carbon atoms at the vertices, should be flat. There is a small number of $sp^3$- and $sp^1$-atoms between the graphene-like layers. In some small areas local graphite clusters are visible, in which the graphene layers are arranged in parallel. In some places of the structure shown in Fig. 2, pores formed. Thus, we can conclude that at a quenching rate of $10^{12}$ K/s and modeling in the $NPT$ ensemble the liquid carbon transforms into heterogeneous porous graphite-like material consisting of randomly arranged graphite clusters and interlaced with graphene layers. When liquid carbon is quenched at a rate of $10^{12}$ K/s, the process of graphitization (the process of formation of structures with $sp^2$-atoms of carbon) is decisive. Since the quenching rate is relatively low, the initial structure of liquid carbon has time to transform into a structure consisting of „mixed" graphene layers of $sp^2$-atoms. At such quenching rates the structures of liquid and $a$-C carbon differ significantly. The authors [49] call such $a$-C structures as amorphous graphene. The structure in Fig. 2, which has a density of 1.93 g/cm$^3$, is visually similar to the structures of $a$-C annealed after quenching (at $\rho = \text{const}$) with a density of 1.5 g/ cm$^3$, the structures were obtained in papers [25,32].

This is due to the fact that annealing of $a$-C gives rise to multiple graphite clusters and graphene layers of carbon atoms with $sp^2$-hybridization. The authors [33], using the GAP potential [27], even at a quenching rate of $10^{14}$ K/s ($\rho = \text{const}$), obtained $a$-C structure in the form of elongated graphite flakes with a density of 1.97 g/cm$^3$. This $a$-C structure was then compared with the structures formed during graphitization while modeling long-term annealing of amorphous structures [50]. The structure shown in Fig. 2 also has much in common with the structure of highly porous $a$-C-carbon obtained from carbides [29].

At the quenching rate of $10^{13}$ K/s and modeling in the $NPT$ ensemble, as can be seen in Fig. 3, a different picture is observed. Although the number of $sp^2$-atoms is quite large (85.1%), as at a quenching rate of $10^{12}$ K/s, neither graphene layers nor graphite clusters are observed in the resulting structure. The structure in Fig. 3 consists of $sp^2$- and $sp^1$-hybridized atoms arranged randomly. The number of $sp^3$-atoms is low (as in Fig. 2), while the number of $sp^1$-atoms increased to 12.1%, which is 3.6 times higher than at the rate $10^{12}$ K/s. At such a quenching rate complete graphitization does not occur, and the quenching rate starts to influence the change in the structure of the resulting $a$-C relative to the structure of liquid carbon. The number of pores in this $a$-C structure is practically the same as in the same as in the $a$-C structure obtained at a quenching rate of $10^{12}$ K/s.

Fig. 4 shows the structure obtained at a rather high quenching rate $10^{14}$ K/s. This structure differs significantly from those considered earlier. Although it still contains a rather large number of $sp^2$-atoms (63.8%), $sp^1$-atoms begin to play a significant role. Their number increases to 34.6%. As can be seen in Fig. 4, $a$-C structure contains

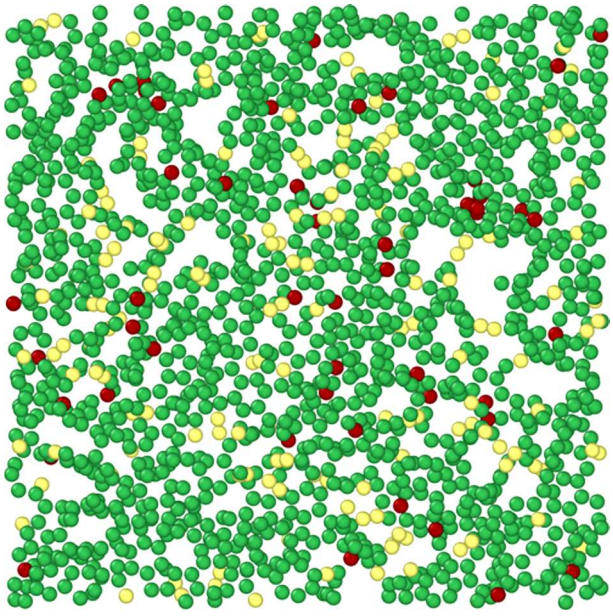

**Figure 3.** Cross section of $a$-C structure for a quenching rate of $10^{13}$ K/s. The structure contains 2.8% of atoms with $sp^3$-, 85.1% of atoms with $sp^2$-, 12.1% of atoms with $sp^1$-hybridization.

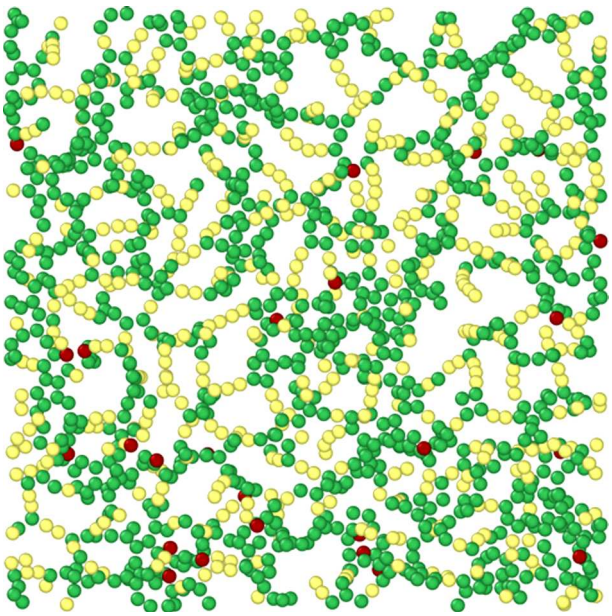

**Figure 4.** Cross section of $a$-C structure for a quenching rate of $10^{14}$ K/s. The structure contains 1.6% of atoms with $sp^3$-, 63.8% of atoms with $sp^2$-, 34.6% of atoms with $sp^1$-hybridization.

a rather large number of carbine-like carbon chains. These chains together with $sp^2$-atoms form a net-structure with a large number of pores or voids, which leads to low density of $a$-C — 1.5 g/cm$^3$. The authors [51] also found a sharp decrease in the density of liquid carbon at a pressure of $P < 1-2$ GPa, believing that this effect is due to the predominance of $sp^1$-chains of atoms and high nanosized porosity. Thus, indeed, at a quenching rate of $10^{14}$ K/s the initial structure of liquid carbon is closer to the structure of the resulting $a$-C than at the rates of $10^{12}$ and $10^{13}$ K/s. In other words, high quenching rates allow partial „freezing“ of the liquid carbon structure in $a$-C. In the paper [20] at a quenching rate of $10^{14}$ K/s in the $NVT$ ensemble and density of 1.2 g/cm$^3$ the number of $sp^1$-atoms in $a$-C was 33%. The authors of [25], modeling the liquid carbon quenching with a density of 1.5 g/cm$^3$ at rates of $10^{15}$ K/s in the $NVT$ ensemble (with subsequent annealing), obtained the content of $sp^1$-atoms in $a$-C from 18 to 37.7%, depending on the type of classical potential used in the calculations. Thus, the ReaxFF potential gives maximum value of 37.7%. On the whole, our calculations of the number of $sp^1$-atoms in $a$-C obtained by quenching are in good agreement with the results of papers [20,25].

## 5. Structural characteristics of amorphous carbon. Short and medium range orders

The study of the structure of amorphous materials is a rather difficult task, since the long range order is absent, and the short range order, although it can be analyzed, is not enough to understand the atomic structure of amorphous solids. For a complete characterization of amorphous materials the additional analysis of the medium range order, which is located beyond the short range order, i.e. beyond the first coordination sphere [52], is required.

For $a$-C model structures, in addition to the density, both short range and medium range orders were analyzed. To characterize the short range order the distribution of carbon atoms by the degree of chemical bond hybridization ($sp$-, $sp^2$-, $sp^3$-), radial and angular distribution functions (RDF and ADF) were calculated. One of the existing methods for studying the medium range order, as it is known from [27,53,54], is the statistical analysis of rings. Note that the structure of the medium range order in $a$-C affects the radial and angular distribution functions.

Fig. 5 shows the RDF for $a$-C structures obtained in our calculations at various quenching rates. The first and second main RDF peaks characteristic for $a$-C [17,23,26] are observed in the vicinity of 1.5 and 2.5 Å. The first peak is associated with short range order and lies within the first coordination sphere. The second peak is located in the second coordination sphere and indicates the presence of medium range order in $a$-C. Unlike liquid carbon, in which the RDF shows a non-zero first minimum at 1.9 Å, in $a$-C for the same point a zero gap between the first and second RDF peaks is clearly visible for all three quenching rates.

The radial distribution function for the quenching rate of $10^{12}$ K/s has a pronounced sharp first peak in the vicinity of 1.46 Å, which corresponds to the chemical bond length for $sp^2$-hybridization in $a$-C. For quenching rates $10^{13}$ and $10^{14}$ K/s this peak decreases and slightly shifts to the right. At a quenching rate of $10^{14}$ K/s the peak amplitude near 1.46 Å is almost two times smaller than for $10^{12}$ K/s. The decrease in the amplitude of this peak is due to the decrease in the content of atoms with $sp^2$-hybridization as the quenching rate increases.

The second main RDF peak in the vicinity of 2.5 Å for the rate of $10^{12}$ K/s has no pronounced asymmetry (characteristic for many amorphous structures). This is most likely due to the features of the medium range order of amorphous graphene. At a rate of $10^{13}$ K/s the structure of the medium range order begins to change. Due to the appearance of the shoulder on the right side, a slight asymmetry of the second peak is noticeable. And at a rate of $10^{14}$ K/s the noticeable asymmetry of the second peak appeared, on the right side of the peak one can see a shoulder that is larger in amplitude than the amplitude of the middle part of the second peak. One can clearly see the influence of the structure change of the medium range order on the RDF form outside the first coordination sphere. Possible reasons for this will be discussed further.

In Fig. 5, within the limits of the short range order, the attention is drawn to the sharp RDF peak near 1.24 Å, the amplitude of which increases with the increase in the quenching rate. A similar peak, but of a small amplitude, is given in the papers [20,24,34]. The authors explain this peak by the presence of atoms with $sp^1$ hybridization

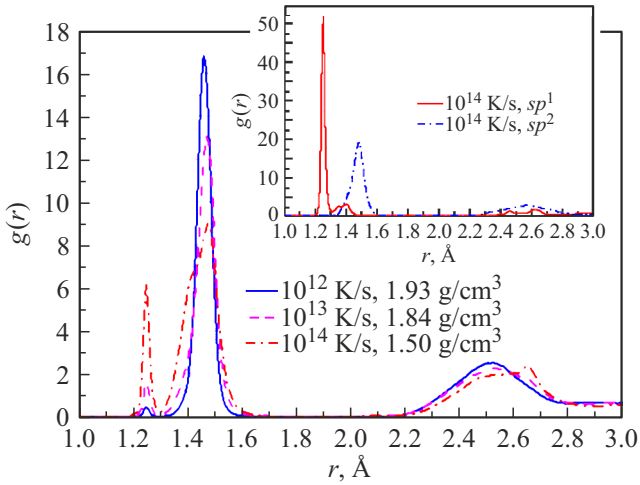


**Figure 5.** *a*-C RDF for quenching rates: $10^{12}$, $10^{13}$, $10^{14}$ K/s. The inset shows the results of the RDF differential analysis separately for $sp^1$ and $sp^2$ atoms at a quenching rate of $10^{14}$ K/s.

in *a*-C structures. This peak is especially noticeable in low-density *a*-C. The fact that the amplitude of this peak in [20,24,34] is small is most likely due to the annealing of carbon amorphous structures after liquid carbon quenching. In the paper [31] for the densities *a*-C 2.2, 1.8 and 1.4 g/cm$^3$ the dependence of the RDF peak amplitude on the density in the vicinity of 1.2 Å (Fig. 5) was identified, and it is similar to that obtained by us.

We, like the authors [20,24,34], associate the peak in the vicinity of 1.24 Å with the presence of carbon atoms with $sp^1$-hybridization, which, as can be clearly seen from Fig. 4, form curved chains in *a*-C. However, in the paper [26] in *a*-C with a low density of 0.5 and 1.0 g/cm$^3$, a small shoulder is seen on the left side of the first RDF peak near 1.2 Å, which the authors attribute to the presence of a small number of triatomic carbon rings. To clarify the situation, for *a*-C structures obtained by us we performed a RDF differential analysis separately for atoms with $sp^1$- and $sp^2$-hybridization.

The result for the quenching rate $10^{14}$ K/s is shown in the inset in Fig. 5. As can be seen in this inset, the RDF for atoms with $sp^1$-hybridization has one pronounced peak near 1.24 Å, which is much larger in amplitude than the other small peaks in the vicinity of 1.4 and 2.5 Å. There is no peak near 1.24 Å on the RDF for atoms with $sp^2$-hybridization, there are the first and second main RDF peaks in the vicinity of 1.5 and 2.5 Åonly. Thus, the increase in the peak amplitude at 1.24 Å with the increase in the quenching rate in Fig. 5 is uniquely associated with the increase in the content of atoms with $sp^1$-hybridization. For the quenching rate of $10^{14}$ K/s the peak at 1.24 Å is approximately equal to 2/3 of the peak maximum at 1.46 Å.

Besides, as can be seen in Fig. 5, at the quenching rate of $10^{14}$ K/s a shoulder appeared on the left side of the peak 1.46 Å. No peaks were found on the separate RDFs for atoms with $sp^1$-hybridization and for atoms with $sp^2$-hybridization that could explain the appearance of this shoulder. We think that this shoulder could appear due to bonds between the chains of atoms with $sp^1$-hybridization with the structures consisting of atoms with $sp^2$-hybridization.

After a detailed description of the short range order it is necessary to investigate the structure of the medium range order for the model *a*-C obtained in our calculations at different quenching rates. Fig. 6 shows the ADF, which is associated not only with the short range, but also with the medium range order. Fig. 7 shows the dependence of the total number of rings divided by the number of atoms in the cell, on the number of atoms in the ring (statistical distribution of rings). This dependence is the key to understanding the structure of the medium range atomic order in *a*-C. Since ADF and a statistical distribution of rings are interconnected through the medium range order structure, we will further jointly discuss the features of the graphs shown in Fig. 6 and 7. ADF characterizes the azimuthal angle formed by triplets of the nearest carbon atoms within the first coordination sphere. The statistical distribution of rings was calculated by us using the shortest path criterion according to the King's diagram [55] in ISAACS program [56]. The calculation procedure is described in detail in [57].

The ADF maxima in Fig. 6 for all three quenching rates are located around 120°, which reflects the defining structural features of one of the crystalline allotropes of carbon — graphite. This angle is typical for atoms with $sp^2$-hybridization in six-atom carbon rings that make up graphite and graphene. As can be seen in Fig. 7, as the quenching rate increases, the ADF maxima decrease with the decrease in the number of hexatomic rings. For a quenching rate of $10^{12}$ K/s the peak near 120° is practically the only one that corresponds to the structure of amorphous graphene shown in Fig. 2. Note that the carbon clusters formation in the form

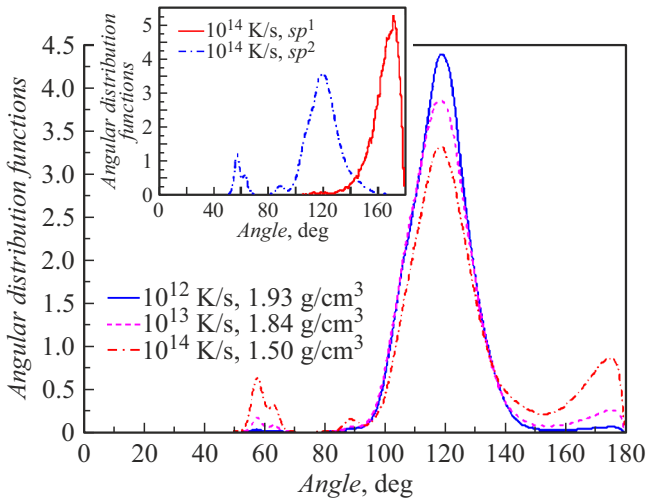


**Figure 6.** ADF of *a*-C for quenching rates: $10^{12}$, $10^{13}$, $10^{14}$ K/s. The inset shows the results of the ADF differential analysis separately for $sp^1$ and $sp^2$ atoms at a quenching rate of $10^{14}$ K/s.

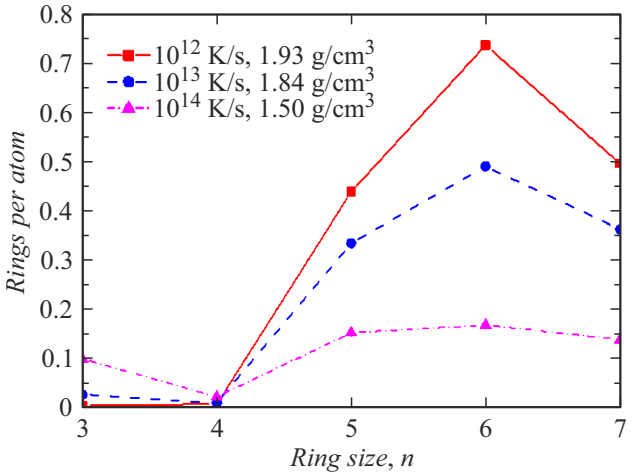


**Figure 7.** Dependence of the total number of rings divided by the number of atoms in the cell, on the number of atoms in the ring for *a*-C structures for quenching rates: $10^{12}$, $10^{13}$, $10^{14}$ K/s.

of hexatomic carbon rings leads, in fact, to the formation of a certain structure precisely within the medium range order, since the distances between non-neighboring atoms in such a ring are greater than the radius of the first coordination sphere.

The peaks in the vicinity of 120° in Fig. 7 for all three quenching rates are quite wide, which is explained by the presence of pentatomic and heptatomic carbon rings in *a*-C. Just these rings form curved (convex and concave) graphene-like layers (Fig. 2) and actively participate in the formation of the medium range order. Also, rings of high orders indirectly indicate structural voids.

As can be seen in Fig. 6, at quenching rates of $10^{13}$ and $10^{14}$ K/s three more peaks are observed in ADF: near 60°, 90° and a wide peak near 175°. The physical nature of 175° peak can be explained from the differential analysis of ADF separately for atoms with $sp^1$- and $sp^2$-hybridization. The result of the analysis for the quenching rate $10^{14}$ K/s is shown in the inset in Fig. 6. The peak in the vicinity of 175° is formed, as can be clearly seen in Fig. 4, due to the presence of numerous bent chains of atoms with $sp^1$-hybridization. Since the curvature of the chains is different, and each curvature corresponds to its own angle, a rather wide peak is formed in ADF, which is blurred at the corners. As the quenching rate increases, the number of $sp^1$-chains in *a*-C increases, as well as the amplitude of this peak increases. In the paper [27] at low densities of *a*-C, i.e. below 2.0 g/cm$^3$, ADF also has wide peak, but with a maximum at 180°, which the authors [27] explain by the presence of almost linear bonds of atoms with $sp^1$-hybridization. In our case, as can be seen from Fig. 4, all chains of *sp*-atoms have a bent shape; accordingly, the ADF graphs in Fig. 6 go to zero at 180°.

A small ADF peak in Fig. 6 in the vicinity of 90° is apparently due to the presence of a certain number of tetratomic carbon rings (as can be seen in Fig. 7). The largest number of tetratomic rings is observed at a quenching rate of $10^{14}$ K/s. According to the authors opinion [27], the asymmetry of the second RDF peak near 2.5 Å, which is a characteristic for the medium range order in many amorphous materials, indicates the presence of tetratomic carbon rings in the *a*-C structure. In other words, the appearance of the shoulder at the second peak of RDF is due to the atoms located along the diagonal of the tetratomic ring. The asymmetry of the second RDF peak (Fig. 5) begins to appear for the quenching rate of $10^{13}$ K/s and is clearly visible at $10^{14}$ K/s due to the increase in the number of tetatomic rings with the increase in the quenching rate.

The ADF peak near 60° in the *a*-C structure occurs, as a rule, at high quenching rates due to the presence of triatomic carbon rings [26,27]. In *a*-C structure with a density of 1.2 g/cm$^3$, obtained by liquid carbon quenching, a rather large number of triatomic carbon rings was observed when calculating by the tight-binding method [20]. In [18] based on the modeling of liquid carbon quenching by the *ab initio* method tetratomic carbon rings were found in the *a*-C structure with a density of 2.0 g/cm$^3$. It is known that triatomic carbon rings are in a very stressed state and are energetically unfavorable structures [33]. For the formation of triatomic carbon rings, as the DFT calculations show [19], a rather large strain energy is required. The question arises how triatomic carbon rings still appear in the *a*-C structure obtained by liquid carbon quenching. Apparently, the thing is that liquid carbon contains both triatomic and tetratomic carbon rings [27]. Moreover, the largest number of such rings [27] is observed just at relatively low densities of liquid carbon: 2.5, 2.0, 1.5 g/cm$^3$. The higher the quenching rate is, the more elements of liquid carbon structure, including highly stressed triatomic carbon rings, will be „frozen“ in *a*-C. During *a*-C annealing, the number of such energetically unfavorable rings will decrease.

Like the authors of [27] we found triatomic and tetratomic rings in the structure of liquid carbon with a density of 1.2 g/cm$^3$. As can be seen from Fig. 7, at a quenching rate of $10^{14}$ K/s the a-C structure contains a rather large number of triatomic rings — more than half of the number of all hexatomic carbon rings. These triatomic rings are responsible for the ADF peak near 60° (Fig. 6). This peak splitting into two local maxima may be due to the fact that among triangles of three carbon atoms, on average, scalene triangles predominate, in which one or two angles are less than 60°.

## Conclusion

As a result of experimental quenching of liquid carbon on a cold diamond substrate, we obtained for the first time a new material — graded amorphous carbon. To this date, the authors are not familiar with any other experimental methods for obtaining the carbon graded material.

As a result of MD modeling of liquid carbon quenching on a cold diamond substrate with actual experimental rates [12] $a$-C model samples were obtained. The use of the $NPT$ ensemble, which, as a rule, is not used to calculate the quenching process in $a$-C production, made it possible to bring the modeling conditions closer to the actual experimental conditions. Therefore, the structures of $a$-C model samples obtained by us should be close in their properties to the structures of actual experimental samples.

The analysis of the density change of liquid and $a$-C with temperature increase at a constant pressure 1 GPa during the quenching process made it possible to determine the moment of $a$-C formation and to estimate the glass transition temperature of liquid carbon at about 3000 K.

As a result of the study of short range and medium range orders, structural features of the graded $a$-C were identified. Structural analysis methods were used, including the calculation of the carbon atoms distribution according to the degree of hybridization of the chemical bond ($sp$-, $sp^2$-, $sp^3$-), RDF, ADF, and statistical analysis of rings.

The calculation of the carbon atoms distribution according to the degree of hybridization confirmed the trend towards the increase in the content of $sp^1$-bonds in amorphous carbon with increase in the quenching rate and decrease in the $a$-C density.

The differential analysis of RDF made it possible to justify the occurrence of a pronounced RDF peak near 1.24 Å, which is due to a significant number of carbon atoms with $sp^1$-hybridization in $a$-C, and the number of atoms increases at high quenching rates $10^{13}$, $10^{14}$ K/s.

As a result of the statistical analysis of the rings and ADF analysis we explain the appearance of the asymmetry of the second RDF peak in $a$-C near 2.5 Å at high quenching rates due to the presence of tetratomic rings. This asymmetry is a characteristic for the medium range order in many amorphous materials

The differential analysis of ADF made it possible to identify the physical nature of the wide peak appearance in the vicinity of 175°, which occurred due to the formation of numerous bent chains of carbon atoms with $sp^1$-hybridization in $a$-C.

The ADF peak in the vicinity of 60° is due to the presence of highly stressed triatomic carbon rings in the $a$-C structure, which initially occurred in high-temperature liquid carbon. When quenched at sufficiently high rates, they do not have time to break down and remain in the resulting $a$-C.

The decrease in the rate of liquid carbon quenching with the distance from the diamond substrate leads to heterogeneity of the $a$-C structure, and thus to the formation of graded $a$-C. Near the diamond substrate $a$-C has a highly porous structure of low density 1.5 g/cm$^3$ with rather high content of curved chains (34.6%) of carbon atoms with $sp^1$-hybridization. Further, with the distance increasing from the substrate, $a$-C gradually transforms into practically completely graphitized carbon containing 95% of atoms with $sp^2$-hybridization, with a density of 1.93 g/cm$^3$, close to the density of graphite, i.e. 2 g/cm$^3$. The structure of such $a$-C is a randomly interlaced graphene-like layers, sometimes such $a$-C is called amorphous graphene.

### Acknowledgments

The results presented in this paper were obtained using the equipment of the Center of Collective Use „JIHT RAS Supercomputer Center “, the „Joint Supercomputer Centre of the Russian Academy of Sciences “and the Shared Resource Centre „Far Eastern Computing Resource IACP FEB RAS “.

### Conflict of interest

The authors declare that they have no conflict of interest.

## References

[1] N.F. Marks. *Amorphous Carbon and Related Materials. In: Computer-Based Modeling of Novel Carbon Systems and Their Properties: Beyond Nanotubes* (Springer, Dordrecht, 2010), DOI: 10.1007/978-1-4020-9718-8_5

[2] H.K. Tran, C.E. Johnson, D.J. Rasky, F.C.L. Hui, M.-T. Hsu, Y.K. Chen. *Phenolic Impregnated Carbon Ablators (PICA) for Discovery Class Missions.* In: 31st AIAA Thermophys. Conf. (New Orleans, 1996), p. 1911. DOI: 10.2514/6.1996-1911

[3] A.S.V. Pulickel, M.B. Chaudhari. Int. J. Appl. Res. Mech. Eng., **1** (3), 1 (2012). DOI: 10.47893/IJARME.2012.1039

[4] Y. Liu, A. Erdemir, E.I. Meletis. Surf. Coatings Technol., **82**, 48 (1996). DOI: 10.1016/0257-8972(95)02623-1

[5] J. Robertson. Mater. Sci. Eng. Reports, **37** (4−6), 129 (2002). DOI: 10.1016/S0927-796X(02)00005-0

[6] H. Tsai, D.B. Bogy. J. Vac. Sci. Technol. A: Vacuum, Surfaces and Films, **5** (6), 3287 (1987). DOI: 10.1116/1.574188

[7] L. Colombo, A. Fasolino. *Computer-Based Modeling of Novel Carbon Systems and Their Properties: Beyond Nanotubes* (Springer, Berlin, 2010), DOI: 10.1007/978-1-4020-9718-8

[8] M. Niino, T. Hirai, R. Watanabe. J. Jpn. Soc. Compos. Mater., **13**, 257 (1987).

[9] P.M. Pandey, S. Rathee, M. Srivastava, P.K. Jain. *Functionally Graded Materials (FGMs). Fabrication, Properties, Applications, and Advancements* (Taylor & Francis Group, LLC, CRC Press, 2022), DOI: 10.1201/9781003097976

[10] J.C. Sung, J. Lin. *Diamond Nanotechnology: Synthesis and Applications* (Jenny Stanford Publishing, NY., 2010), DOI: 10.1201/9780429066498

[11] A.Y. Basharin, V.S. Dozhdikov, V.T. Dubinchuk, A.V. Kirilin, I.Y. Lysenko, M.A. Turchaninov. Tech. Phys. Lett., **35**, 428 (2009). DOI: 10.1134/S1063785009050137

[12] V.S. Dozhdikov, A.Yu. Basharin, P.R. Levashov. High Temperature, **60** (2), S248 (2022). DOI: 10.31857/S0040364421050045

[13] V.S. Dozhdikov, A.Yu. Basharin, P.R. Levashov. J. Physics: Conf. Series, **653** (1), 012091 (2015). DOI: 10.1088/1742-6596/653/1/012091

[14] V.S. Dozhdikov, A.Yu. Basharin, P.R. Levashov. J. Physics: Conf. Series, **1147** (1), 012008 (2019). DOI: 10.1088/1742-6596/1147/1/012008

[15] G. Galli, R.M. Martin, R. Car, M. Farrinello. Phys. Rev. Lett., **62** (5), 555 (1989). DOI: 10.1103/PhysRevLett.62.555
[16] C.Z. Wang, K.M. Ho. Phys. Rev. Lett., **71** (8), 1184 (1993). DOI: 10.1103/PhysRevLett.71.1184
[17] N.A. Marks, D.R. McKenzie, B.A. Pailthorpe, M. Bernasconi, M. Parrinello. Phys. Rev. Lett., **76** (5), 768 (1996). DOI: 10.1103/PhysRevLett.76.768
[18] D.G. McCulloch, D.R. McKenzie, C.M. Goringe. Phys. Rev. B, **61** (3), 2349 (2000). DOI: 10.1103/PhysRevB.61.2349
[19] N.A. Marks, N.C. Cooper, D.R. McKenzie, D.G. McCulloch, P. Bath, S.P. Russo. Phys. Rev. B, **65** (7), 075411 (2002). DOI: 10.1103/PhysRevB.65.075411
[20] C. Mathioudakis, G. Kopidakis, P.C. Kelires, C.Z. Wang, K.M. Ho. Phys. Rev. B, **70** (12), 125202 (2004). DOI: 10.1103/PhysRevB.70.125202
[21] T. Kumagai, S. Hara, J. Choi, S. Izumi, T. Kato. J. App. Phys., **105** (6), 064310 (2009). DOI: 10.1063/1.3086631
[22] Z.D. Sha, P.S. Branicio, Q.X. Pei, V. Sorkin, Y.W. Zhang. Comput. Mater. Sci., **67**, 146 (2013). DOI: 10.1016/j.commatsci.2012.08.042
[23] L. Li, M. Xu, W. Song, A. Ovcharenko, G. Zhang, D. Jia. Appl. Surf. Sci., **286**, 287 (2013). DOI: 10.1016/j.apsusc.2013.09.073
[24] L.J. Peng, J.R. Morris. Carbon, **50** (3), 1394 (2012). DOI: 10.1016/j.carbon.2011.11.012
[25] C. de Tomas, I. Suarez-Martinez, N.A. Marks. Carbon, **109**, 681 (2016). DOI: 10.1016/j.carbon.2016.08.024
[26] R. Ranganathan, S. Rokkam, T. Desai, P. Keblinski. Carbon, **113**, 87 (2017). DOI: 10.1016/j.carbon.2016.11.024
[27] V.L. Deringer, G. Csanyi1. Phys. Rev. B, **95** (9), 094203 (2017). DOI: 10.1103/PhysRevB.95.094203
[28] P. Rowe, V.L. Deringer, P. Gasparotto, G. Csanyi, A. Michaelides. J. Chem. Phys., **153** (3), 034702 (2020). DOI: 10.1063/5.0005084
[29] M.W. Thompson, B. Dyatkin, H.W. Wang, C.H. Turner, X. Sang, R.R. Unocic, C.R. Iacovella, Y. Gogotsi, A.C.T. van Duin, P.T. Cummings. J. Carbon Research, **3** (4), 32 (2017). DOI: 10.3390/c3040032
[30] X. Li, A. Wang, K.-R. Lee. Comput. Mater. Sci., **151**, 246 (2018). DOI: 10.1016/j.commatsci.2018.04.062
[31] K. Li, H. Zhang, G. Li, J. Zhang, M. Bouhadja, Z. Liu, A.A. Skelton, M. Barati. J. Chem. Theory Comput., **14** (5), 2322 (2018). DOI: 10.1021/acs.jctc.7b01296
[32] C. de Tomas, A. Aghajamali, J.L. Jones, D.J. Lim, M.J. Lopez, I. Suarez-Martinez, N.A. Marks. Carbon, **155**, 624 (2019). DOI: 10.1016/j.carbon.2019.07.074
[33] R. Jana, D. Savio, V.L. Deringer, L. Pastewka. Modelling Simul. Mater. Sci. Eng., **27** (8), 085009 (2019). DOI: 10.1088/1361-651X/ab45da
[34] Q. Liu, L. Li, Y.R. Jeng, G. Zhang, C. Shuai, X. Zhu. Comput. Mater. Sci., **184**, 109939 (2020). DOI: 10.1016/j.commatsci.2020.109939
[35] B. Bhattarai, D.A. Drabold. Carbon, **115**, 532 (2017). DOI: 10.1016/j.carbon.2017.01.031
[36] N. Orekhov, G. Ostroumova, V. Stegailov. Carbon, **170**, 606 (2020). DOI: 10.1016/j.carbon.2020.08.009
[37] N.A. Marks. Phys. Rev. B., **56** (5), 2441 (1997). DOI: 10.1103/PhysRevB.56.2441
[38] L.M. Mejía-Mendoza, M. Valdez-Gonzalez, Jesús Muñiz, U. Santiago, A.K. Cuentas-Gallegos, M. Robles. Carbon, **120**, 233 (2017). DOI: 10.1016/j.carbon.2017.05.043
[39] L. Alonso, J.A. Alonso, M.J. López. *Computer Simulations of the Structure of Nanoporous Carbons and Higher Density Phases of Carbon. In: Many-body Approaches at Different Scales* (Springer, Cham., Catania, 2018), DOI: 10.1007/978-3-319-72374-7_3
[40] J.C. Palmer, K.E. Gubbins. Microporous and Mesoporous Mater., **154**, 24 (2012). DOI: 10.1016/j.micromeso.2011.08.017
[41] V.S. Dozhdikov, A.Yu. Basharin, P.R. Levashov, D.V. Minakov. J. Chem. Phys., **147** (21), 214302 (2017). DOI: 10.1063/1.4999070
[42] L. Liu, Yi. Liu, S.V. Zybin, H. Sun, W.A. Goddard III. J. Phys. Chem. A, **115** (40), 11016 (2011). DOI: 10.1021/jp201599t
[43] A.C. van Duin, S. Dasgupta, F. Lorant, W.A. Goddard III. J. Phys. Chem. A, **105** (41), 9396 (2001). DOI: 10.1021/jp004368u
[44] S.B. Kylasa, H.M. Aktulga, A.Y. Grama. J. Comput. Phys., **272**, 343 (2014). DOI: 10.1016/j.jcp.2014.04.035
[45] S. Plimpton. J. Comp. Phys., **117** (1), 1 (1995). DOI: 10.1006/jcph.1995.1039 (https://lammps.sandia.gov/index.html)
[46] N.A. Marks, D.R. McKenzie, B.A. Pailthorpe, M. Bernasconi, M. Parrinello. Phys. Rev. B, **54** (14), 9703 (1996). DOI: 10.1103/PhysRevB.54.9703
[47] S. Best, J.B. Wasley, C. de Tomas, A. Aghajamali, I. Suarez-Martinez, N.A. Marks. C.-J. Carbon Research, **6** (3), 50 (2020). DOI: 10.3390/c6030050
[48] D.R. McKenzie, A.R. Merchant, D.G. McCulloch, H. Malloch, N.A. Marks, M.M.M. Bilek. Surf. Coat. Technol., **198** (1–3), 212 (2005). DOI: 10.1016/j.surfcoat.2004.10.043
[49] B. Bhattarai, P. Biswas, R. Atta-Fynn, D.A. Drabold. Phys. Chem. Chem. Phys., **20** (29), 19546 (2018). DOI: 10.1039/C8CP02545B
[50] R.C. Powles, N.A. Marks, D.W.M. Lau. Phys. Rev. B, **79** (7), 075430 (2009). DOI: 10.1103/PhysRevB.79.075430
[51] N. Orekhov, M. Logunov. Carbon, **192**, 179 (2022). DOI: 10.1016/j.carbon.2022.02.058
[52] Y. Hiraokaa, T. Nakamuraa, A. Hirataa, E.G. Escolara, K. Matsueb, Y. Nishiuraa. Proc. Natl. Acad. Sci. U.S.A., **113** (26), 7035 (2016). DOI: 10.1073/pnas.152087711
[53] Y. Shi, J. Neuefeind, D. Ma, K. Page, L.A. Lamberson, N.J. Smith, A. Tandia, A.P. Song. J. Non-Cryst. Solids, **516**, 71 (2019). DOI: 10.1016/j.jnoncrysol.2019.03.037
[54] V.L. Deringer, N. Bernstein, A.P. Bartók, M.J. Cliffe, R.N. Kerber, L.E. Marbella, C.P. Grey, S.R. Elliott, G. Csanyi. J. Phys. Chem. Lett., **9** (11), 2879 (2018). DOI: 10.1021/acs.jpclett.8b00902
[55] S.V. King. Nature, **213** (5081), 1112 (1967). DOI: 10.1038/2131112a0
[56] S. Le Roux, V. Petkov. J. Appl. Cryst. **43** (1), 181 (2010). DOI: 10.1107/S0021889809051929
[57] S. Le Roux, P. Jund. Comput. Mater. Sci., **49** (1), 70 (2010). DOI: 10.1016/j.commatsci.2010.04.023

*Translated by I.Mazurov*